Published in IET Electric Power Applications
Received on 13th August 2010
Revised on 26th October 2010
doi: 10.1049/iet-epa.2010.0193

ISSN 1751-8660

An adaptive controller for the novel planar switched reluctance motor

J.F. Pan[1] *N.C. Cheung*[2]

[1]*Department of Automation, College of Mechatronics and Control Engineering, Shenzhen University, Shenzhen, Guangdong Province, People's Republic of China*
[2]*Department of Electrical Engineering, The Hong Kong Polytechnic University, Hung Hom, Kowloon, Hong Kong*
E-mail: eencheun@polyu.edu.hk

Abstract: This paper proposes an adaptive control method for the planar switched reluctance motor (PSRM). Regarding to the mechanical deficiencies and control problems that exist in the prototype, a new machine with compact size and improved performance has been built. Following a brief simulation with finite element analysis (FEA), detailed adaptive controller design with online parameter identification is performed. Experimental results prove that the controller has good position control performance over PID algorithm in dynamic, static and robustness to disturbances. It is expected that the novel two-dimensional (2D) direct-drive machine with adaptive control strategy find its potential use in industrial applications.

1 Introduction

High-precision two-dimensional motions are in high demand for the advanced manufacture industry. Traditionally, two axes of perpendicular motion are often accomplished by two pairs of rotary motors coupled with mechanical rotary-to-linear translators stacked on top of each other, such as the $X-Y$ table. This method has the disadvantage of accumulated error from each axis of the motion's mechanics and the system's precision is dependent on the mechanical couplers. With the fast development of power electronics and control algorithms, there is a tendency of 'simplifying the mechanics through improved control strategy'. This paves the way for the usage of direct-drive machines. In a direct-drive system, such as the linear motor, the mechanical output of the machine is directly coupled to the machine load, thus eliminating any mechanical translator, such as pulley, belt or gear. With the direct coupling method, the mechanical structure is greatly simplified and the whole system is easier to assemble, reduced in cost and increased in performance. However, efficiency is affected in direct-drive machines due to the larger air gaps and the edge effects inherent in direct-drive actuators. Therefore direct-drive systems have never been a competitive replacement for applications with high force or high speed outputs. However, direct-drive machines can still find applications in the high-precision processes, owing to its simplified mechanical structure.

A direct-drive planar motor based on switched reluctance (SR) principle has been developed in [1]. Considering previous work, single or dual proportional–integral–derivative (PID) control techniques are attempted on the prototype. However, unbalanced dynamic response and static backlash errors exist for each axis of motion [2]. Since the motor encounters mechanical imperfections and disturbances during its operation, an adaptive controller should be introduced for the correction of mechanical defections and control disturbances. Therefore in this paper, after the optimisation for mechanical structure and motor construction, the authors propose a controller based on indirect adaptive control strategy with online parameter estimation. The paper structure is arranged as follows. First the mechanical improvement and motor construction are discussed in Section 2. Following that a brief finite-element (FE) analysis is given in Section 3, and Section 4 focuses on modelling and controller design for the planar motor. Section 5 discusses dynamic and static performance for each axis of motion and conclusion remarks are given in Section 6.

2 Mechanical improvements and motor construction

The planar switched reluctance motor (PSRM) can be considered as a pair of perpendicularly interconnected linear switched reluctance motors (LSRM) with the motor pitch arranged as the 'straightened-out' version of two 6/4-pole SR motors along both X and Y directions. The operation of the moving platform is at the same height for each axis of motion. This corresponds to an integrated actuator capable of two perpendicular directions of motion at the same time. The PSRM has many advantages such as simple structure, high robustness, low cost and free from mechanical maintenance, and so on. However, due to severe non-linear characteristics inherent in the magnetic path for SR machines, proper linearisation and control scheme should be introduced [3].

From the previous prototype discussed in [4], the authors find that the X-axis with a high mass and the pair of linear bar slides impose a heavy burden for Y-axis movement.

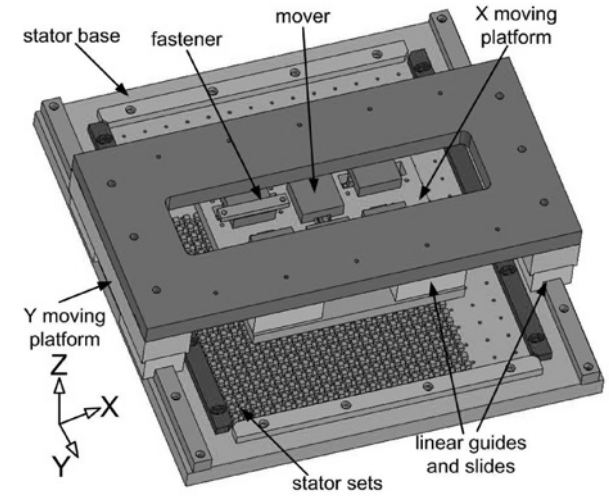

Fig. 1 *Improved structure with compact size and high stiffness*
a Mechanical structure of the PSRM
b Motor picture

Since the movers are fixed under the moving platform with screws, there is a tendency of shape distortion when activated, which may influence the effective air gap between the moving platform and stator base. An improved structure with compact size and high stiffness is proposed and developed as shown in Fig. 1. The following mechanical improvements can be summarised as

1. A pair of high-grade linear guides with 'suspension installation' are fixed as the moving path for *X*-axis;
2. Six movers are locked tight to the platform to prevent attraction movements between movers and stator sets when excited;
3. All silicon-steel sheets are held with laser welding instead of holes with screws to achieve a better magnetic circulation path.

The mechanical and electrical parameters are listed in Table 1.

3 FE analysis of the PSRM

For pre-analysis of motor performance and preparation for implementation of control strategies, three-dimensional (3D) FE analysis is performed to explore the coupling effect and propulsion force output with a FE analysis package. The 3D model is constructed according to specifications listed in Table 1.

Table 1 Motor parameters

pole pitch	9 mm
pole width	4.5 mm
pole slot	4.5 mm
air gap	0.2 mm
number of turns per phase	160
size of base plate	340 × 350 mm^2
travel distance	100 (*X*) × 180 (*Y*) mm^2
size of moving platform (*Y*)	180 × 360 mm^2
encoder precision	1 μm

3.1 Test of mutual inductance

Mutual inductance effect between any two movers is first inspected. If the coupling effect is negligible, the procedure of FE modelling can be simplified with just one mover relative to corresponding stator sets, since all six movers have the same dimensions and ratings. Moreover, there is no need for any decoupling mechanism involved in the control algorithm. To precisely represent the problem, a 3D model with one mover and its closest neighbour is constructed and the flux density contour is analysed at 1000 N A. As shown in Fig. 2, magnetic flux distribute within the short magnetic path along the activated mover, stator sets and the air gap in between. This is because the magnetic path between the two adjacent movers has relatively large reluctance as air.

3.2 Propulsion force calculation

The 2D propulsion force profile of one mover to the stator is calculated according to different positions within one pole-pitch with respect to different current levels as shown in Fig. 3. At lower excitations below 1000 N A when the motor operates in unsaturated region, maximum force occurs at half pole-teeth positions at 2.25 mm with sinusoidal-like curves. At higher current levels, the waveforms become distorted such that force climbs to the peak earlier before half pole-teeth positions under saturated region with more end and edge affects.

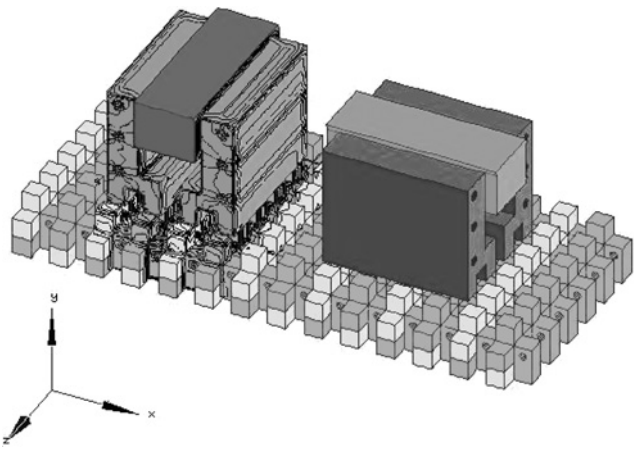

Fig. 2 *Flux distribution of the PSRM*

doi: 10.1049/iet-epa.2010.0193

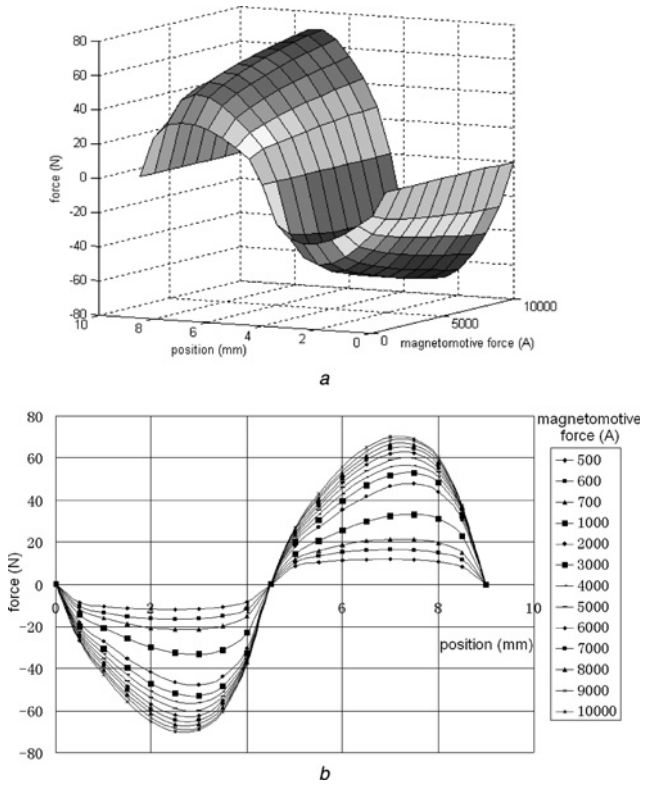

Fig. 3 *Force calculation from FEM*

a 3D
b 2D

4 Adaptive controller design

4.1 Mathematic model of the PSRM

For one axis of motion, the mechanical equations that governs the dynamic system can be described as [4]

$$M_{x(y)}S''_{x(y)} + B_{vx(y)}S'_{x(y)} + f_l = F_{x(y)} \tag{1}$$

where $F_{x(y)}$ is the total force of X- or Y-axis required, $M_{x(y)}$ and $B_{vx(y)}$ is mass and friction coefficient of X- or Y-axis, f_l is the total load force impressed on the moving platform. Symbol $x(y)$ stands for X-axis or Y-axis.

From the electrical side, any axis of motion can be characterised with the voltage balance equations as [5]

$$V_{kx(y)} = R_{kx(y)}i_{kx(y)} + \frac{\mathrm{d}\lambda_{kx(y)}(S_{x(y)}, i_{kx(y)})}{\mathrm{d}t} \tag{2}$$

where $V_{kx(y)}$, $R_{kx(y)}$, $i_{kx(y)}$ and $S_{kx(y)}$ is terminal voltage, coil resistance, current and position. Generally $\lambda_{kx(y)}$ is the total flux-linkage and can be regarded as the sum of self, mutual and leakage flux-linkages. For the PSRM, as mentioned before, mutual flux-linkage can be regarded as negligible.

From SR principles, propulsion force is represented in common form as

$$F_{kx(y)}(x(y), i_k) = \frac{1}{2} \times \frac{\mathrm{d}L_{kx(y)}}{\mathrm{d}x(y)} i^2_{kx(y)}, \quad k = 1, 2, 3 \tag{3}$$

From the above characterisation (1)–(3) for the PSRM, it can be concluded that each axis of motion behaves like a highly non-linear relationship between force and current. Therefore a linearisation scheme should be introduced for the derivation of current at designated force command. Considering computation complexity, the force distribution function (FDF) described in [6] is applied for each axis of motion.

For the control of PSRM, each axis of motion can be considered as a dual-loop control scheme for a single-input single-output system when force total command $F_{x(y)}$ is system input and position $S_{x(y)}$ as system output. Since the control system is filled with noise under real-time operation, the second-order system can be represented in discrete time form as [7]

$$A(z^{-1})S_{x(y)} = B(z^{-1})F_{x(y)} + v \tag{4}$$

where $A(z^{-1})$ and $B(z^{-1})$ are polynomials to be determined and

$$\begin{cases} A(z^{-1}) = 1 + a_1 z^{-1} + a_2 z^{-1} \\ B(z^{-1}) = b_1 + b_2 z^{-1} \end{cases} \tag{5}$$

4.2 Online parameter estimation

The purpose of parameter estimation is to correctly identify parameters a_1, a_2, b_1 and b_2 that contain all motor information for one axis. Even though disturbances may enter at any place into the control system with any form, for the Nth estimation, it can be considered as stochastic errors in least-square form as [7]

$$S^N_{x(y)} = \phi^N_{x(y)}\boldsymbol{\theta} + e^N \tag{6}$$

where $\boldsymbol{\theta} = [a_1 a_2 b_1 b_2]$, $\phi^N_{x(y)} = [-S^{N-1}_{x(y)}, -S^{N-2}_{x(y)}]$ and e is residuals. Parameter vector $\boldsymbol{\theta}$ can be estimated by RLS algorithm as [7]

$$\begin{cases} \hat{\theta}^{N+1}_{x(y)} = \hat{\theta}^{N}_{x(y)} + G^N_{x(y)}[S^{N+1}_{x(y)} - (\phi^{N+1}_{x(y)})^{\mathrm{T}}\hat{\theta}^{N}_{x(y)}] \\ G^N_{x(y)} = \dfrac{P^N_{x(y)}}{\rho + (\phi^{N+1}_{x(y)})^{\mathrm{T}}P^N_{x(y)}\phi^{N+1}_{x(y)}} \\ P^{N+1}_{x(y)} = \dfrac{1}{\rho}[I - G^{N+1}_{x(y)}(\phi^{N+1}_{x(y)})^{\mathrm{T}}]P^N_{x(y)} \end{cases} \tag{7}$$

where $\boldsymbol{P}$ is the covariance matrix and $\boldsymbol{G}$ is gain matrix. ρ is forgetting factor that reflects the relationship between converging rate and tracking ability according to previous data. For initial value of $\boldsymbol{P}$, $\boldsymbol{P} = \sigma\boldsymbol{I}$ as $\sigma = 20$ and $\boldsymbol{I}$ is 4×4 unit matrix. The program termination criterion for recursive calculation can be set as

$$\left| \frac{\hat{\theta}^{N+1}_{x(y)} - \hat{\theta}^{N}_{x(y)}}{\hat{\theta}^{N}_{x(y)}} \right| < \varepsilon \tag{8}$$

where ε is a small positive number. Equation (8) denotes that if the maximum proportion of error from the last and present is comparatively small, it can be considered the present value is the correct estimate.

4.3 Adaptive controller design

The adaptive controller is designed based on pole-placement method with the structure as shown in Fig. 4, with the control equation as $Ru(t) = TF_{x(y)}(t) - MS_{x(y)}(t)$ and R, T, M are the polynomials to be determined. The causality conditions should be satisfied as deg $M \leq R$ and deg $T \leq R$. The closed-loop control output and system output can be represented as [8]

$$\begin{cases} S_{x(y)} = \dfrac{B(z^{-1})T(z^{-1})}{A(z^{-1})R(z^{-1}) + B(z^{-1})M(z^{-1})} \\ \qquad \times F_{x(y)} + \dfrac{B(z^{-1})M(z^{-1})}{A(z^{-1})R(z^{-1}) + B(z^{-1})M(z^{-1})} \times v \\ u = \dfrac{B(z^{-1})T(z^{-1})}{A(z^{-1})R(z^{-1}) + B(z^{-1})M(z^{-1})} \\ \qquad \times F_{x(y)} - \dfrac{B(z^{-1})M(z^{-1})}{A(z^{-1})R(z^{-1}) + B(z^{-1})M(z^{-1})} \times v \end{cases} \tag{9}$$

and the closed-loop characterisation equation is represented as

$$AR + BS = A_c = A_0 A_m \tag{10}$$

with causality conditions satisfied

$$\begin{cases} \deg A_c \geq 2\deg A - 1 \\ \deg A_m - \deg B_m \geq \deg A - \deg B \end{cases} \tag{11}$$

where A_m and B_m is polynomials that contain desired closed-loop poles and zeros. The goal of pole-placement design is to specify the desired closed-loop poles so that system output perfectly tracks the input command. Since external disturbance is relatively low to the input command signals, the disturbance can be assumed to satisfy the following conditions as [9]

$$(q-1)v(t) = \xi(t) \tag{12}$$

where q is forward shift operator and $\xi(t)$ is white noise.

For the cancellation of disturbance, R should contain $q - 1$ as

$$R(z^{-1}) = (q-1)R'(z^{-1}) \tag{13}$$

If polynomials R, M and T satisfy the following equations

$$\begin{cases} R(q) = (q-1)R'(q) = X(q)R^0(q) + S_{x(y)}(q)B(q) \\ M(q) = X(q)M^0(q) - S_{x(y)}(q)A(q) \\ T(q) = X(q)T^0(q) \end{cases} \tag{14}$$

where R^0, M^0 and T^0 are solutions of [9], the system output

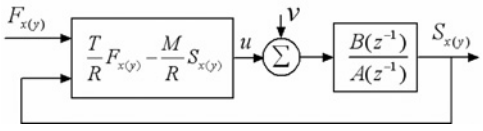

Fig. 4 *Controller structure*

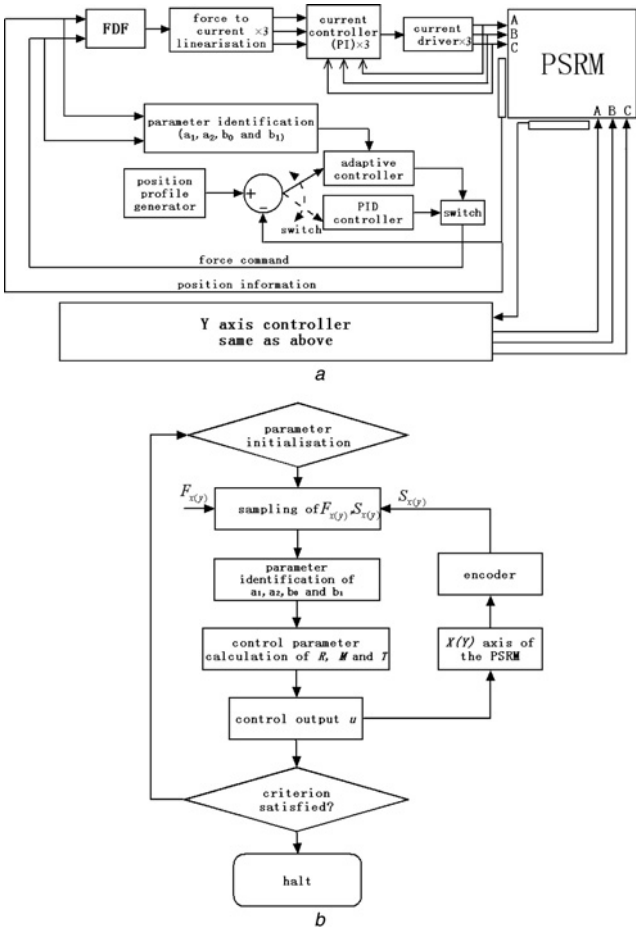

Fig. 5 *Control diagram and flowchart*

then becomes

$$S_{x(y)}(t) = \frac{X(q)A_0(q)B_m(q)}{X(q)A_0(q)A_m(q)} \times F_{x(y)}(t) + \frac{B_m(q)R'(q)}{X(q)A_0(q)A_m(q)} \times \xi(t) \tag{15}$$

From (15), it can be concluded that system output is capable of tracking input command in the desired manner and insensitive to external disturbance. The control diagram and flowchart is shown in Fig. 5.

5 Experimental results

The control experiment is conducted on the platform of a dSPACE DS1104 controller card. This card has an on-board 250 MHz digital signal processor and two 24-bit digital encoder channels that interface the encoders from each axis of motion. Six digital-to-analogue converters are used for current reference output for the current drivers. The control card can directly interface with real-time workshop and MATLAB and control parameters can be modified online. Fig. 6 shows the overall experimental setup. Since the outer position loop bandwidth is much slower than that of the current loop, a sampling rate of 10 and 1 KHz is selected for the outer position and inner current control loop, respectively.

Since the motor is not capable of self-start under adaptive control method, PID control is utilised for closed-loop position control and online parameter identification. After parameter estimation process is finished, the control

doi: 10.1049/iet-epa.2010.0193

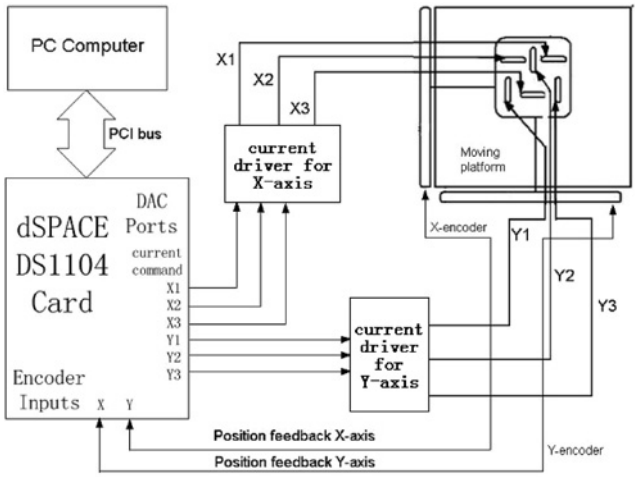

Fig. 6 *Experimental setup*

algorithm is switched to adaptive method as shown in Fig. 5*a*. Table 2 lists the expected poles, zeros, forgetting factors and PID parameters for each axis. Since disturbances from *X*-axis are more complicated with the suspended slides structure, the forgetting factor is bigger than that of *Y*-axis with more useful information from new data. For a smooth motor operation in real conditions, the input signal is set as S-profile with amplitude of 20 mm and frequency of 0.3 Hz.

5.1 Parameter identification

Parameter identification process starts after PID control has achieved a stable output performance. As shown in Fig. 7 of the estimated parameters, it can be seen that it takes 3–5 s for convergence to stable values. Since mechanical structures are not identical from each axis of motion, corresponding system parameters differ between *X* and *Y*-axis. Although different operation conditions may lead to different parameter identification results, the estimation mechanism proves effective for the PSRM. After the identification process is stable, adaptive control can be implemented to replace PID method.

5.2 Control performance

The dynamic response of adaptive control is shown in Fig. 8. To clearly demonstrate the difference between the two control methods, wave curves are drawn in the same figure with the same time base. For different control cycles, the performance under PID method is not uniform. The response from *X*-axis is even worse since the mechanical structure is more complex which could bring more disturbances compared with that from *Y*-axis. As can been seen from the figure, overshoot only appears in the third

Table 2 Parameters for pole placement and PID

Parameters	*X*-axis	*Y*-axis
a_{m1}	−1.936	−1.932
a_{m2}	0.938	0.936
b_{m0}	−0.850	−0.800
b_{m2}	−0.800	−0.800
ρ	0.999	0.99
P	2.5	2.0
D	35	20

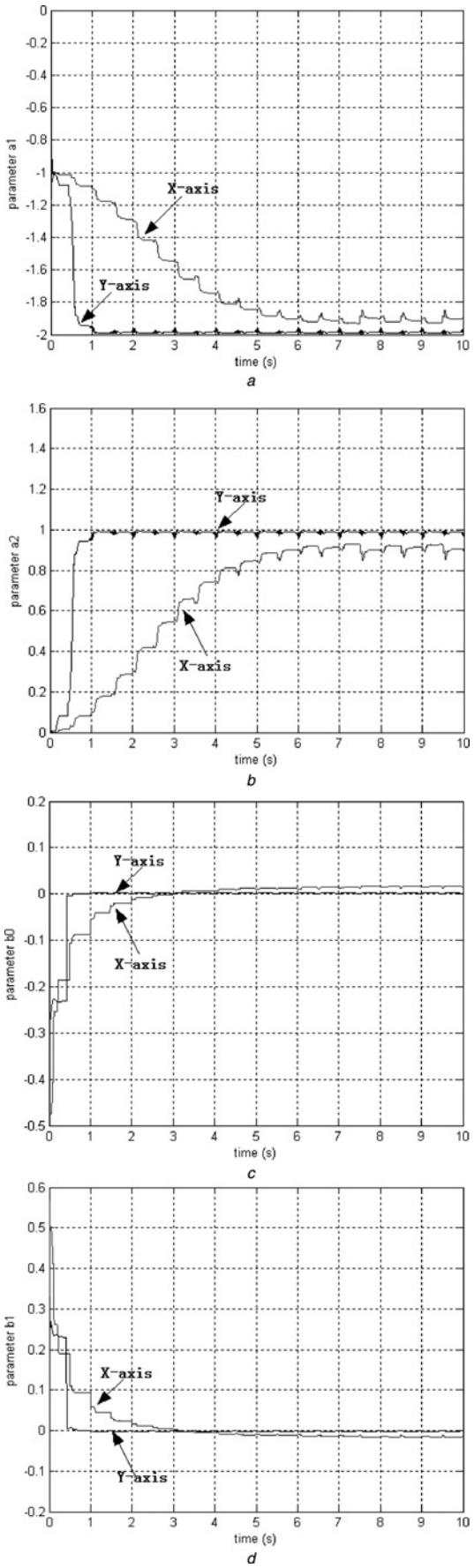

Fig. 7 *Parameter identification results*

a Parameter a_1
b Parameter a_2
c Parameter b_0
d Parameter b_1

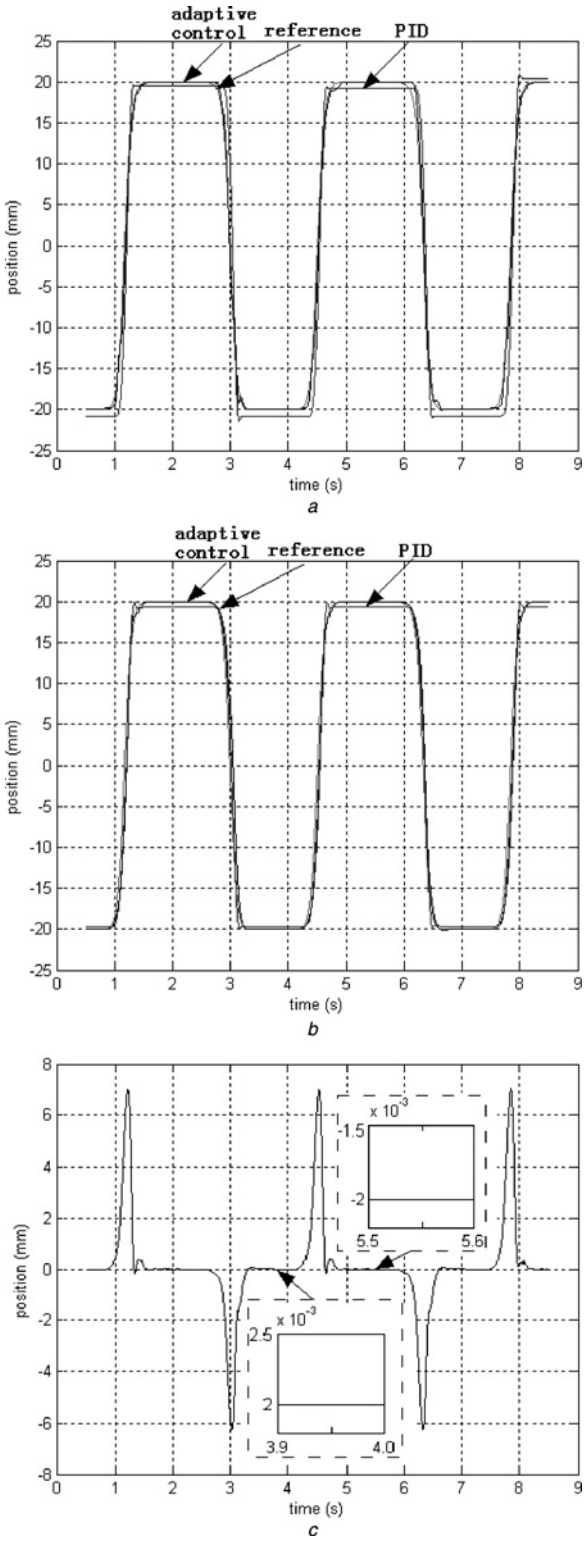

Fig. 8 *Dynamic response*

a *X*-axis
b *Y*-axis
c Dynamic error response

control cycle for *X*-axis and at each constant state of ± 20 mm, each cycle has different static response with large static errors. However, from adaptive control, the motor is capable of uniform performance for both dynamic and static responses. Although the rise time may vary from each cycle, it proves that the control algorithm is capable of regulation from parameter or disturbance interference to achieve a comparatively more optimised response under the requirement of expected poles.

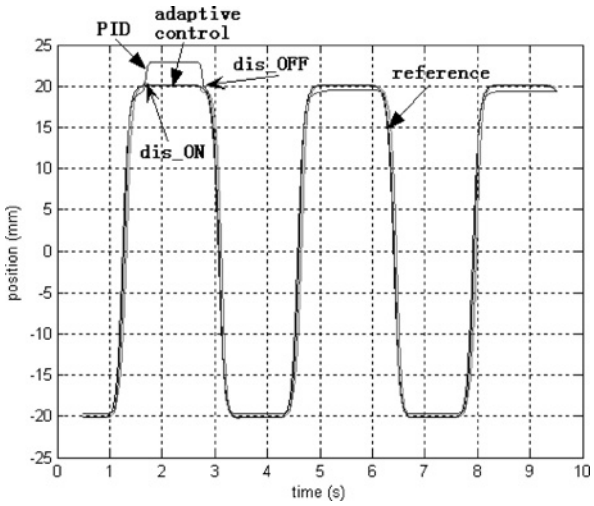

Fig. 9 *Response from force disturbance with 10 N*

For *Y*-axis of motion, the dynamic response from PID is quite unsymmetrical from both sides of motor operation. However, the adaptive control algorithm can effectively correct this problem. For static response, the control algorithm is capable of achievement of static precision of ± 2 μm as shown in Fig. 8*c*.

5.3 Response with disturbances

To further test the difference between the two control algorithms, experiments towards disturbances are carried out. The position reference signal and all control parameters remain unchanged and a force disturbance of 10 N from the output of FDF block for the *Y*-axis as shown in Fig. 5*a* is included on the control system. As shown in Fig. 9 the response from PID and adaptive control, PID is not capable of regulation as the disturbance takes effect and it responds with a large position disparity. However, the adaptive control only has slight overshoot when the disturbance is applied and disengaged.

For imitation of continuous external load influence, a spring with the coefficient of 57.5 N/m is connected to the *Y* moving platform. The spring expands and contracts at each side of movement. As illustrated in Fig. 10 the

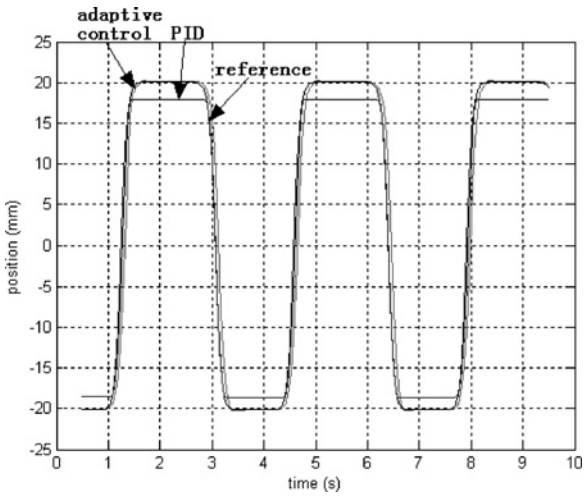

Fig. 10 *External disturbance response with a spring*

doi: 10.1049/iet-epa.2010.0193

response from both control algorithms, it can be seen that only the adaptive control method is able to correct such disturbance from both spring expansion and contraction and provide a reasonable static response at the same time under time-variant disturbances.

6 Conclusion

An adaptive controller with online parameter identification is implemented on the improved PSRM with a compact size and robust mechanical structure. From the experimental results, the control method has the capability to correct mechanical imperfections and adapts to disturbances with considerable dynamic and static precision over PID control method. With the implementation of the proposed control method, the authors believe that the 2D direct-drive machine will find many potential applications in the high-precision manufacture area.

7 Acknowledgments

The authors would like to thank the National Natural Science Foundation of China and Hong Kong Research Grants Council for the sponsoring of this research project under the project code 51007059 and PolyU 5140/07E; the authors would also like to thank Guangdong Natural Science Fund 2008225 and Shenzhen Government fund 08cxy-29 for their support.

8 References

1 Cheung, N.C., Pan, J.F., Yang, J.M.: 'Two-dimensional variable reluctance planar motor'. US Patent 7,170,203
2 Pan, J., Cheung, N.C., Yang, J.M.: 'High-precision position control of a novel planar switched reluctance motor', *IEEE Trans. Ind. Electron.*, 2005, **52**, (6), pp. 1644–1652
3 Krishnan, R.: 'Switched reluctance motor drives: modeling, simulation, analysis, design, and applications' (CRC Press, Boca Raton, FL, 2001)
4 Pan, J.: 'A 2D variable reluctance planar motor'. PhD thesis, The Hong Kong Polytechnic University, Hong Kong, 2007
5 Miller, T.J.E.: 'Switched reluctance motor and their control' (Magnet Physics Publishing and Clarendon Press, Oxford, 1993)
6 Pan, J.F., Cheung, N.C., Gan, W.C., Zhao, S.W.: 'A novel planar switched reluctance motor for industrial applications', *IEEE Trans. Magn.*, 2006, **42**, (10), pp. 2836–2839
7 Ljung, L.: 'System identification – theory for the user' (Prentice-Hall, 1999, 2nd edn.)
8 Åström, K.J., Wittenmark, B.: 'Adaptive control' (Addison-Wesley, 1995)
9 Huang, C.-I., Fu, L.-C.: 'Adaptive approach to motion controller of linear induction motor with friction compensation', *IEEE Trans. Mechatron.*, 2007, **12**, (4), pp. 480–490